PCCP

PAPER

View Article Online
View Journal | View Issue

Cite this: *Phys. Chem. Chem. Phys.*, 2025, **27**, 17959

Excited-state dynamics of cinnamate-based UV filters: bringing decay pathways to light by photoelectron velocity map imaging

Ivan Romanov,[a] Wim Roeterdink,[a] Yorrick Boeije,[abc] Hugo Maurer[a] and Wybren Jan Buma *[ad]

Received 12th June 2025,
Accepted 4th August 2025

DOI: 10.1039/d5cp02240a

rsc.li/pccp

Cinnamic acids and cinnamates are attracting considerable interest as starting point for the rational development of novel UV filters. Key to their optimization is a fundamental understanding of the nonradiative processes that occur after photon absorption. Here we employ kinetic-energy-resolved photoelectron spectroscopy to uncover the deactivation mechanisms occurring after photoexcitation of a series of substituted cinnamates. We find that the recorded photoelectron spectra (i) confirm and extend conclusions on pathways involving the triplet manifold previously obtained indirectly, (ii) provide insight into the electronic structure of the excited singlet manifold, and (iii) elucidate the influence of substituents on their photodynamics. In addition, they have allowed for the determination of accurate ionization energies that so far had not been determined.

1. Introduction

Photons provide a source of energy that can be used advantageously in many molecule-based applications. However, for such applications the absorption of the photon is only an initial step that normally is followed by a myriad of consecutive steps in which this photon energy is transformed into other forms of energy. Eminent examples are found in photosynthesis where photon energy is transformed into chemical energy,[1,2] and molecular nanotechnology where photons power molecular motors by transforming photon energy into mechanical energy.[3–5] Another class of materials revolves around the absorption of light and dissipating its energy into thermal energy. UV filters used in artificial and naturally occurring sunscreens are well-known examples.[6] Since the main function of these filters is to absorb harmful UV light and protect the skin from sun damage, the generated thermal energy is considered more as a by-product than as the primary objective. On the other hand, there are currently also extensive efforts to develop materials specifically aimed to bring the generated heat to use.[7] One of the more recent developments in that area are so-called molecular heaters to be used in agri- and horticulture where they would serve on the one hand to enhance crop growth, but also protect crops from extreme cold weather.[8]

In an ideal world photon energy is completely converted into thermal energy. In practice, however, there are competing detrimental pathways that reduce the efficiency of this conversion, and, more importantly, may lead to undesired side reactions. Especially for applications in which health safety is an important factor it is therefore imperative to determine the pathways along which the absorbed energy is converted into thermal energy. Illustrative in this respect is 2-ethylhexyl-4-methoxycinnamate (EHMC) used in commercial sunscreens as a UV-B blocker for which it was shown[9] that a long-lived electronically excited state is involved in the excited-state dynamics of the photon-absorbing electronically excited state, thereby rationalizing the observation that reactive oxygen species are generated upon prolonged irradiation.[10,11]

EHMC is one of the UV-B filters that have cinnamic acid as their basic backbone. Being a naturally occurring and therein employed compound, it has been an attractive starting point for the further development and optimization of such filters.[12–24] The observation of a long-lived electronically excited state thus spurred significant efforts to come to a further understanding of the nature of this state and its decay pathways. Seminal work of Ebata *et al.*[25–29] based on ionization efficiency spectra and quantum chemical calculations of relaxation pathways involving minimum energy surface crossings led to the conclusion that the triplet manifold is at the origin of the observed long-lived signals.

[a] *University of Amsterdam, Van 't Hoff Institute for Molecular Sciences, Science Park 904, 1098 XH Amsterdam, The Netherlands. E-mail: w.j.buma@uva.nl*
[b] *Department of Chemical Engineering and Biotechnology, University of Cambridge, Philippa Fawcett Drive, Cambridge CB3 0AS, UK*
[c] *Department of Physics, Cavendish Laboratory, University of Cambridge, JJ Thomson Avenue, Cambridge CB3 0HE, UK*
[d] *Radboud University, Institute for Molecules and Materials, FELIX Laboratory, Toernooiveld 7c, 6525 ED Nijmegen, The Netherlands*

The molecular beam studies that so far have been employed to elucidate the spectroscopy and dynamics of the electronically-excited state manifold of cinnamic-acid based UV filters have either used mass-resolved ion detection in Resonance Enhanced MultiPhoton Ionization (REMPI) spectroscopic studies or emission-based detection techniques in Laser Induced Fluorescence (LIF) studies. Further insight and confirmation of the contribution of the various excited-state decay pathways can be obtained from kinetic-energy-resolved photoelectron spectroscopy. In such studies not only the presence of ions is detected, but also their internal energy. Since the electronic and vibrational state of the generated ions directly reports on the electronic structure and dynamics of the state from which ionization took place, such studies are key to elucidating the pathways along which photon energy is dissipated.[30]

In the present study we apply to this purpose velocity map imaging (VMI) of photoelectrons in one- and two-colour REMPI spectroscopic studies of a series of substituted cinnamates. These cinnamates have been chosen such that they feature different aspects inferred previously to be relevant for the excited-state dynamics of substituted cinnamates. In combination with quantum chemical calculations these studies aim to provide further confirmation and understanding of the role of the triplet manifold and the potential energy surfaces involved, as well as provide insight into the electronic structure of the manifold of electronically excited singlet states that is responsible for UV-B absorption. Understanding and harnessing these pathways will not only enhance the design of more efficient materials but also contribute to their broader applications.

2. Methods

2.1. Experimental

Experiments have been performed in a newly constructed molecular beam spectrometer that allows for time-of-flight mass spectrometry (TOF-MS), electron velocity map imaging (VMI) as well as ion VMI. In this setup the molecular beam is created with an injector assembly that consists of a stainless steel oven in which a glass container with the sample is placed and kept at a temperature at which the sample of interest has a high enough vapour pressure. For the present molecular systems this was found to be 140–160 °C. The oven is connected to a pulsed valve (General Valve Iota One) equipped with a 0.4 mm diameter conical nozzle that is kept 5–10 °C higher in temperature to avoid clogging. Typically, pulse durations of 180–220 μs were used. In the present experiments a supersonic expansion of the molecule of interest is generated by leading neon at a backing pressure of 2 bar through the oven and expanding the resulting gas mixture through the nozzle into the vacuum chamber.

After passing through a conical skimmer with a diameter of 2 mm the molecular beam enters the ion source region which is equipped with a modified version of the three-plate electrostatic lens system originally designed by Parker and Eppink[31] that closely resembles the system used in the coincidence setup designed by Janssen and coworkers.[32] The lens directs electrons to a Photonis microchannel plate (MCP) detector equipped with a phosphor screen measuring 40 mm in diameter that is situated 160 mm from the ionisation site. Alternatively, by reversing the polarity of the lens, ions are steered into a 600 mm long time-of-flight (TOF) tube where they are detected using a 18 mm dual microchannel plate detector (Jordan Co. C-701) although VMI detection is also possible by exchanging this detector with the Photonis detector. Images are acquired using the Micro-Manager 2.0[33] plugin in conjunction with an Andor CMOS camera. These images are further processed and analysed using the NumPy[34] and PyAbel[35] packages within a Python 3.10[36] environment.

In the present study both one-colour (1 + 1) as well as two-colour (1 + 1′) Resonance Enhanced Two-Photon Ionization (RE2PI) experiments have been performed. Although in both types of experiments laser intensities were reduced as much as possible to avoid non-resonant contributions to the signal, some background contributions remained inevitable. For the (1 + 1) experiments off-resonance images were therefore recorded under the same excitation conditions as the on-resonance images and subsequently subtracted from the on-resonance images. For the (1 + 1′) experiments, on the other hand, a background correction was performed using both the images acquired for the resonant (1 + 1) signal under the same laser intensity conditions as used to record the (1 + 1′) image, as well as images obtained under non-resonant (1′ + 1′) conditions. The processed and averaged images were subjected to an Abel transformation using the rBASEX[37] algorithm implemented in the PyAbel package. The slice through the reconstructed 3D photoelectron distribution that results from such a transformation then gives access to an angle-integrated photoelectron spectrum and photoelectron angular distribution. For the present experiments the energy scale of the recorded photoelectron spectra was calibrated using (3 + 1) REMPI transitions of Xe for which a $\Delta E/E$ resolution of about 3% was obtained.

The one- and two-colour R2PI experiments have been performed using a frequency-doubled Sirah Cobra-Stretch dye laser operating on DCM and pumped by a Spectra Physics Lab-190 Nd:YAG laser. In the two-colour R2PI experiments, ionisation was achieved using a Neweks PSX-501 ArF excimer laser (193 nm, 6.42 eV). In order to extract a polarized laser beam from the latter laser, a Laseroptik thin film polariser was employed. This beam was focussed using a lens with a 1 m focal length to reduce the interaction volume of this laser beam with the molecular beam and the ionisation chamber. The polarisation of both laser beams was parallel to the plane of the MCP detector. Typical excitation and ionisation energies were less than 10 μJ.

Methyl ferulate and methyl coumarate (methyl-4-hydrocinnamate) were used as purchased from Sigma Aldrich, while methyl sinapate and sinapoyl methyl lactate were synthesized in house using synthetic routes as described in the SI.

2.2. Theoretical

For each of the molecules shown in Fig. 1 calculations have been performed on the adiabatic and diabatic ionization

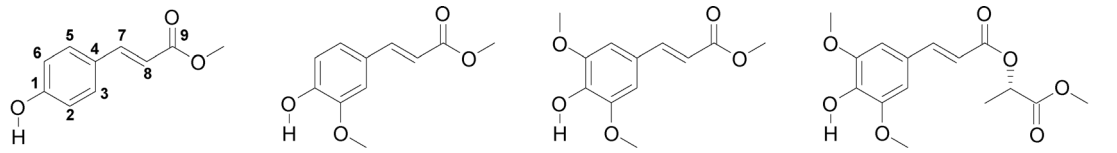

Fig. 1 Cinnamates studied and employed atom numbering. Drawn are the *syn*/*cis* conformers.

energies from (i) the ground state S_0, (ii) the first electronically excited singlet state S_1 and (iii) the lowest electronically excited triplet state T_1 of the neutral molecule to the ground state D_0 of the cation as well as its first and second electronically excited states D_1 and D_2. To this purpose the geometries of S_0, D_0, and T_1 were optimized with (Unrestricted) Density Functional ((U)DFT) at the ωB97XD/cc-pVDZ level[38,39] while for the electronically excited states of the neutral and cation Time-Dependent DFT (TD-DFT) was employed to optimize their geometries. Previous studies on cinnamates[25–29,40] have found that the potential energy surface of T_1 features energy minima at both a planar conformation as well as conformations with a nearly perpendicular geometry of the $C_7{=}C_8$ double bond (see Fig. 1 for atom numbering). In the present study similar observations were made. In the following we will distinguish between these planar and twisted conformations by referring to them as T_{1p} and T_{1t}, respectively. The energies obtained for the various electronic states at their equilibrium geometry allowed for the calculation of adiabatic ionization energies, while vertical ionization energies were obtained from (TD)-UDFT calculations of the energies of the ionic states at the equilibrium geometries of the electronic state of interest of the neutral molecule. All calculations have been performed using the Gaussian16, Rev. C.02 suite of programs.[41]

3. Results and discussion

As discussed in the introduction, the present study aims to elucidate the pathways along which S_1 decays after being excited, and, in particular, the extent to which other electronically excited states are involved in these pathways. Photoelectron spectra obtained for ionization *via* S_1 offer in principle such an insight but their interpretation hinges on the assignment of the bands observed in these spectra to particular ionization pathways, which in turn critically depends on the accuracy with which adiabatic and -in particular-vertical ionization energies can be predicted. In the present study we face in this respect a number of challenges. Firstly, the calculation of ionization energies from S_1 requires accurate energies of D_0. However, it is well known that the error in such values can easily be of the order of a few tenths of eV.[42] Similar uncertainties occur for the prediction of the energies of the electronically excited states of the ion from TD-DFT calculations that are necessary to obtain ionization energies to D_1 and D_2. Secondly, identification of a triplet-mediated decay pathway requires accurate ionization energies from T_1 for which an accurate value of its excitation energy is needed, but also for this excitation energy the same kind of uncertainty can be expected. In passing by we notice that our experiments are performed under isolated molecule conditions in which energy is conserved. A potential triplet mediated decay pathway will thus populate highly-excited vibrational levels of T_1 after intersystem crossing from S_1. We assume that efficient ionization of such levels occurs under conservation of vibrational energy, that is, upon ionization highly-excited vibrational levels of an ionic state are populated.

In the present study we have therefore applied a two-pronged approach based on one- and two-colour R2PI. The excitation energy of the vibrationless level of S_1 of the compounds studied here turns out to be slightly larger than half of their D_0 adiabatic ionization energy. As a result, one-colour (1 + 1) R2PI *via* the $S_1 \leftarrow S_0$ 0-0 transition leads to photoelectron spectra from which the adiabatic ionization energy associated with ionisation of the vibrationless level of S_0 to the vibrationless level of D_0 can be determined with an accuracy of about 1–5 meV depending on the amount of energy that is released in the photoelectrons. We then correlate these experimental data with our computational results by correcting the calculated D_0 adiabatic and vertical ionization energies to match the experimentally observed adiabatic ionization energy. In practice it was found that our calculations tend to underestimate the ionization potential and that a correction of 0.3 ± 0.1 eV needs to be applied. Adiabatic and vertical ionization energies from the vibrationless ground state to the electronically excited D_1 and D_2 states of the ion were then determined by using the calculated (TD)-UDFT excitation energies of these states with respect to the experimentally determined D_0 adiabatic ionization energy.

In a second step we use two-colour (1 + 1′) R2PI using 193 nm photons to ionize the molecule after that it has been excited to the vibrationless level of S_1. From an energy point of view the total energy that is absorbed by the molecule is sufficient to allow ionization to D_0, D_1, as well as D_2 although vibrational overlap considerations restrict for electronically excited states other than S_1 the ionization efficiency to the electronically excited states of the ion (*vide infra*). While one-colour (1 + 1) ionization of highly-excited vibrational levels of T_1 populated *via* intersystem crossing after excitation of the vibrationless level of S_1 is thus highly improbable, two-colour (1 + 1′) R2PI experiments allow for efficient ionization of such levels. We calculate kinetic energies of photoelectrons associated with

this ionization pathway by using the corrected energy of D_0 (see above) at the optimized geometry of T_1, and take for the vibrational energy in the triplet the energy difference between the optimized S_1 and T_1 states. A similar approach could also be used for the ionization energies of T_1 to the electronically excited D_1 and D_2 states of the ion, but it turns out that the vertical ionization energies of T_1 to these states are considerably higher than the total energy absorbed in a $(1 + 1')$ process with 193 nm. Efficient ionization of T_1 to these ionic states is therefore not possible.

To close this part of the discussion we recall that the molecules studied here feature both planar as well as twisted energy minima in T_1. Ionization of these structures will give rise to photoelectrons with significantly different kinetic energies since the vertical ionization energy of the twisted structure is considerably higher than that of the planar one. In fact, the results presented below will demonstrate that the vertical ionization energy of T_{1t} is too high to allow for efficient ionization of its vibrational levels. However, previous calculations[28] have shown that the energy barrier between T_{1p} and T_{1t} is considerably smaller than the amount of vibrational energy stored in the triplet manifold after intersystem crossing from S_1. The vibrational wavefunctions at these energies are thus effectively spread out over both twisted as well as planar geometries. We therefore assume that the kinetic energies associated with ionization of T_1 can be taken as the ones calculated for T_{1p}.

3.1. Methyl sinapate

The spectroscopic and dynamic properties of methyl sinapate (MS) have in the past been studied extensively using various high-resolution laser spectroscopies based on LIF and REMPI techniques.[15,43,44] Nanosecond pump–probe studies revealed a long-lived decay component that was ascribed to ionization of T_1,[43] a conclusion that was further supported by wavelength dependent ionization efficiency measurements.[44] As already touched upon in the introduction, the most unambiguous evidence for the involvement of the triplet manifold would come, however, from photoelectron spectra in which the various ionization pathways are directly visible. A further advantage of studies on MS is that zero-kinetic-energy-pulsed field ionization (ZEKE-PFI) studies have enabled a very accurate determination of the adiabatic ionization energies of the three conformers that are present under adiabatic expansion conditions.[44] In the following we focus on the predominant *syn*/*cis* conformer for which an adiabatic ionization threshold of 7.4752 ± 0.0001 eV has been determined since for the *anti*/*cis* conformer very similar results have been obtained.

Fig. 2 displays the photoelectron (PE) spectrum obtained for ionization of *syn*/*cis* MS after excitation of the vibrationless level of the S_1 state at 31 059.8 cm^{-1} (3.8509 eV), the arrow indicating the kinetic energy expected for adiabatic ionization to the vibrationless level of D_0 on the basis of the ZEKE-PFI studies (0.226 eV). In first instance it would appear that this value is slightly different from the experimental spectrum in which the first discernible band has a maximum at 0.211 ± 0.005 eV.

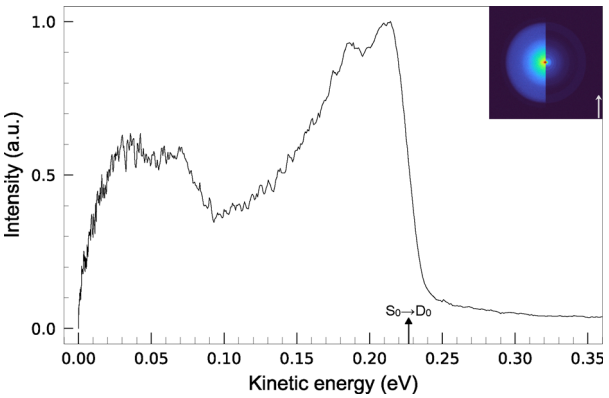

Fig. 2 PE spectrum of the *syn*/*cis* conformer of methyl sinapate obtained after one-colour (1 + 1) R2PI *via* the $S_1 \leftarrow S_0$ 0-0 transition at 310 59.8 cm^{-1}. The arrow indicates the value of the kinetic energy expected from the adiabatic ionization energy determined by ZEKE-PFI.[44] The inset shows in the left half the recorded image while the right half presents the reconstructed slice through the centre of the original 3D distribution with the arrow indicating the electric field polarisation of the laser pulse.

However, it should be taken into account that the ZEKE-PFI spectrum shows -in agreement with theoretical predictions- an extensive progression of a $\sim$60 cm^{-1} low-frequency bending mode with the second and third overtone having the highest intensity. The resolution in the VMI photoelectron spectrum is not high enough to resolve this progression. We therefore expect an unresolved overlap of these bands that will lead to a band shape with a maximum displaced by about 15 meV from the adiabatic ionization energy. This is in excellent agreement with our experimental observations. Inspection of the Franck–Condon activity observed in the ZEKE-PFI spectrum and the activity predicted for higher vibrational levels than shown in ref. 44 leads to the conclusion that the asymmetric shape of the 0.21 eV band and the band at 0.05 eV in the PE spectrum can similarly be well explained by unresolved $D_0 \leftarrow S_1$ Franck–Condon activity upon ionization. One aspect we draw attention to, however, is the partially resolved band at about 0.188 ± 0.005 eV as for one-colour (1 + 1) R2PI of sinapoyl methyl lactate a similar feature is observed.

The PE spectrum obtained for ionization of the same excited-state level in a two-colour $(1 + 1')$ R2PI experiment with 193 nm to ionize the molecule is shown in Fig. 3 in which also the kinetic energies for various ionization pathways are indicated. Since we know the adiabatic $D_0 \leftarrow S_0$ ionization energy from our ZEKE-PFI studies[44] and have determined from the previously discussed one-colour (1 + 1) R2PI VMI image the vertical $D_0 \leftarrow S_1$ ionization energy, these ionization pathways lead to bands at well-determined kinetic energies. However, for other ionization pathways we can only predict kinetic energies on the basis of our calculations which inherently are accompanied by an uncertainty that can easily be of the order of $\pm$ 0.2–0.3 eV.

The kinetic energy distribution in Fig. 3 is characterized by an asymmetric band in the 2.0–2.6 eV region (band I), a band around 1.3 eV (band II) and a low kinetic energy band up to

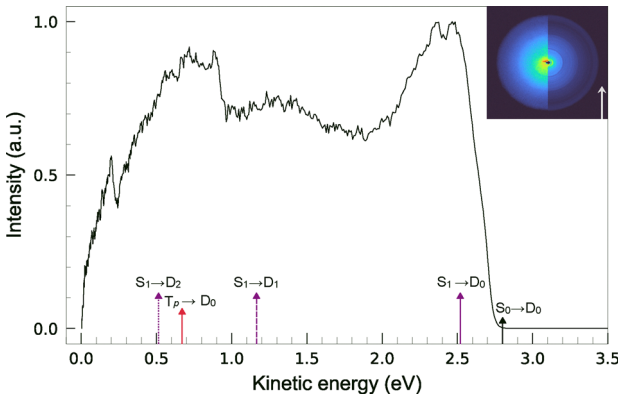

Fig. 3 PE spectrum of the *syn*/*cis* conformer of methyl sinapate obtained after two-colour (1 + 1′) R2PI *via* the $S_1 \leftarrow S_0$ 0-0 transition at 31059.8 cm^{-1} and using a 193 nm photon for ionization. The inset shows in the left half the recorded image while the right half presents the reconstructed slice through the centre of the original 3D distribution with the arrow indicating the electric field polarisation of the counter-propagating excitation and ionization laser pulses. The kinetic energy associated with adiabatic $D_0 \leftarrow S_0$ ionization as determined in ZEKE-PFI studies[44] is indicated with the black solid arrow. Kinetic energies associated with transitions for electronically excited states are indicated by coloured arrows: purple for vertical ionization from the S_1 state, red for vertical ionization from the T_{1p} state. Line styles represent transitions to different states: solid lines to D_0, dashed lines to D_1, and dotted lines to D_2.

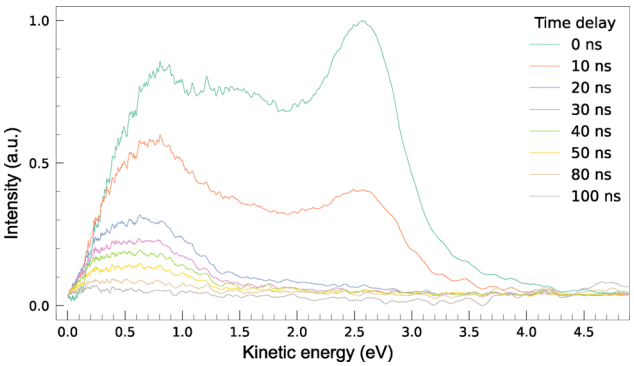

Fig. 4 PE spectrum of the *syn*/*cis* conformer of methyl sinapate obtained after two-colour (1 + 1′) R2PI *via* the $S_1 \leftarrow S_0$ 0-0 transition at 31059.8 cm^{-1} and using a 193 nm photon for ionization for various delays between excitation and ionization laser pulses.

0.9 eV (band III). Band I clearly is associated with the $D_0 \leftarrow S_1$ ionization pathway. It is useful to notice that the energy difference between the $D_0 \leftarrow S_0$ energies and the maximum of band I is to a good approximation equal to the relaxation energy of S_1, that is, the difference between the vertical and adiabatic excitation energies of S_1. Experimentally we thus find a relaxation energy of 0.31 eV, which is in good agreement with the theoretically predicted value of 0.27 eV.

On the basis of our calculations we assign band II to ionization of S_1 to the lowest excited ionic state D_1. Such an assignment find unambiguous support in PE spectra that have been recorded in (1 + 1′) R2PI experiments in which the ionization laser is delayed with respect to the excitation laser and that are shown in Fig. 4.

From this Figure it is clear that the intensities of bands I and II are reduced similarly when the delay time is increased, while band III remains for all practical purposes unaffected. The S_1 state of MS is characterized by the HOMO(π) → LUMO(π^*) excitation, and is historically designated as the V($\pi\pi^*$) state. D_0 and D_1, on the other hand, have dominant contributions from the removal of an electron from the HOMO and HOMO−1, respectively. Electronic propensity rules would then lead one to expect that ionization of S_1 occurs predominantly to D_0. Although band I is indeed more intense than band II, the observation of the latter is interesting and might be indicative for vibronic coupling of S_1 to S_2, which has a dominant (HOMO−1)(π) → LUMO(π^*) contribution and historically has been designated as the V′($\pi\pi^*$) state. On the other hand, a contribution of the $HOMO^0LUMO^1$ configuration to the D_1 wavefunction would also enable ionization from S_1 to D_1.

Band III could in principle arise from ionization of S_1 to D_2 and/or from ionization of T_{1p} to D_0. The delay dependence of the PE spectrum 4 demonstrates, however, that this band is primarily associated with the latter pathway. In view of the presence of multiple energy minima on the potential energy surface of T_1, it would be highly interesting to see whether the PE spectra could provide evidence of -and further information on- these minima. Calculations predict, however, that the vertical ionization energy of T_{1t} to D_0 lies about 0.5 eV above the energies reached by (1 + 1′) absorption. Moreover, as discussed previously, we expect that at the internal energies populated by ISC from S_1 the vibrational wavefunctions of T_1 are spread out and cover both the twisted as well as the planar geometries. Even at higher ionization energies it would thus seem quite a challenging task to interpret a PE spectrum in terms of contributions of these conformations.

PE spectra obtained for (1 + 1) and (1 + 1′) ionization *via* the $S_1 \leftarrow S_0$ 0-0 transition of the *anti*/*cis* conformation of MS at 31170.1 cm^{-1} are reported in the SI (Fig. S_1 and S_2). These spectra are quasi identical to those obtained for the *syn*/*cis* conformer discussed above. The adiabatic ionization energy determined from the (1 + 1) spectrum is in good agreement with the value determined from ZEKE-PFI experiments[44] (7.4846± 0.0001 eV), while the (1 + 1′) spectrum shows the same ionization pathways as observed for the *syn*/*cis* conformer. We therefore conclude that as far as ionization pathways -and thus excited-state composition and decay pathways- these two conformers do not show major differences.

3.2. Sinapoyl methyl lactate

SML features on the phenyl side of the molecule the same substitution pattern as MS, but has the methoxy group of the but-2-enoate part replaced by the more extended methyl lactate. Previous studies identified two conformers and assigned these to the *syn*/*cis* and *anti*/*cis* conformations.[15] Similar to MS, we find that the (1 + 1) and (1 + 1′) PE spectra obtained for these two conformers are nearly identical. In the following we will therefore discuss the results obtained for the *syn*/*cis* conformer and report PE spectra of the *anti*/*cis* conformer of SML in the SI (Fig. S3 and S4).

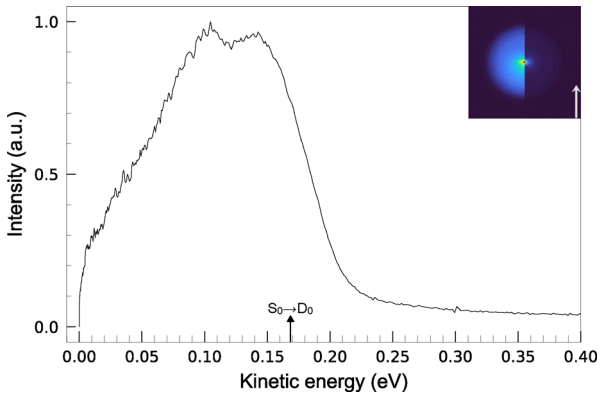

Fig. 5 PE spectrum of the *syn*/*cis* conformer of sinapoyl methyl lactate obtained after one-colour (1 + 1) R2PI *via* the $S_1 \leftarrow S_0$ b_0^1 transition at 30 760 cm^{-1}. The black arrow is the value of the kinetic energy taken to be associated with adiabatic $D_0 \leftarrow S_0$ ionization. The inset shows in the left half the recorded image while the right half presents the reconstructed slice through the centre of the original 3D distribution with the arrow indicating the electric field polarisation of the laser pulse.

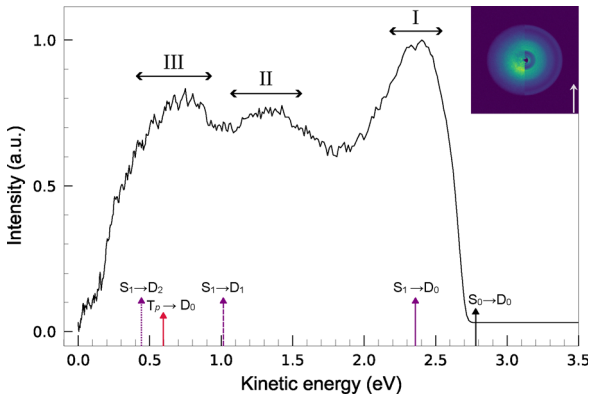

Fig. 6 PE spectrum of the *syn*/*cis* conformer of sinapoyl methyl lactate obtained after two-colour (1 + 1′) R2PI *via* the $S_1 \leftarrow S_0$ b_0^1 transition at 30 760 cm^{-1} and using a 193 nm photon for ionization. The inset shows in the left half the recorded image while the right half presents the reconstructed slice through the centre of the original 3D distribution with the arrow indicating the electric field polarisation of the counter-propagating excitation and ionization laser pulses. The kinetic energy associated with adiabatic $D_0 \leftarrow S_0$ ionization as determined from the one-colour PE spectrum is indicated with the black solid arrow. Kinetic energies associated with transitions for electronically excited states are indicated by coloured arrows: purple for vertical ionization from the S_1 state, red for vertical ionization from the T_{1p} state. Line styles represent transitions to different states: solid lines to D_0, dashed lines to D_1, and dotted lines to D_2.

Fig. 5 displays the PE spectrum obtained for one-colour (1 + 1) R2PI ionization *via* the $S_1 \leftarrow S_0$ b_0^1 transition of the *syn*/*cis* conformer at 30 760 cm^{-1}, mode b corresponding to the C_4–C_7=C_8 bending mode.[15] This transition was taken instead of the 0-0 transition as the signal intensity *via* the 0-0 transition was not high enough. This spectrum resembles to a large extent the PE spectrum obtained for MS, albeit that it is shifted by about 0.05 eV to lower kinetic energies as a result of which the 0.05 eV band observed for MS is quite probably outside the accessible range of kinetic energies. Interestingly, we observe on the high-energy side of the band two partially resolved bands at 0.103 ± 0.010 and 0.141 ± 0.010 eV, thereby mirroring our observations for MS where a similar feature was observed. In view of the similarity of SML and MS we assume that the adiabatic $D_0 \leftarrow S_0$ ionization energy is displaced by the same amount from the maximum of the highest-energy band at 0.0158 eV. Taking also into account that we are ionizing from the b^1 level in S_1, we find for the adiabatic $D_0 \leftarrow S_0$ ionization energy a value of 7.459 ± 0.020 eV, which within the experimental uncertainties is the same as found for MS.

The PE spectrum obtained after (1 + 1′) R2PI ionization is shown in Fig. 6. In view of the electronic similarity between MS and SML we expect *a priori* that their (1 + 1′) PE spectra will closely resemble each other as is indeed confirmed by the experiments that show three bands. Based on the dependence of these bands on the delay between excitation and ionization lasers (not shown) we can conclude that band I in the 2.0–2.7 eV and band II in the 1.0–1.9 eV regions are associated with ionization of S_1 to D_0 and D_1, respectively, while the low-energy band III below 1.0 eV is assigned to ionization from T_{1p} to D_0. From the energy difference between band I and the adiabatic ionization energy of D_0 we conclude that the relaxation energy of S_1 upon excitation from S_0 is in first approximation 0.38 eV, which is -as would have been expected- close to the value found for MS. A more detailed inspection of Fig. 6 shows with respect to band II that the observed vertical $D_1 \leftarrow S_1$ ionization energy is very similar to what is observed for MS. The calculations reproduce in this respect the experiments less well as they predict a value that is about 0.2 eV higher. Although somewhat on the high side, such a deviation is still within the uncertainty one may expect for TD-UDFT excitation energies used to calculate the ionisation energies of electronically excited states of the ion, in particular for low-lying electronically excited states. Band III, on the other hand, is nicely reproduced by the calculations.

The similarity of the (1 + 1′) PE spectra of MS and SML suggests for both molecules a similar triplet quantum yield. Such a conclusion is confirmed by time-resolved (1 + 1′) R2PI decay curves in which the ion yield at the mass of the molecular ion is monitored as a function of the delay between excitation and ionization lasers (see Fig. S5). These traces show a similar ratio for the contributions of the fast and slow decay components assigned to decay of S_1 and T_1, respectively, as observed for MS.

In previous studies on sinapoyl malate (SM) and its derivatives it was observed that the R2PI spectrum of SM displays a broad featureless absorption. It was hypothesized that this might be due to coupling of S_1 with a nearby excited state with charge-transfer character that was assumed to be the $^1n\pi^*$ state. Support for such an explanation was found in the photon fluence dependence of the excitation spectrum of SML. In the present study we confirm these observations: (1 + 1) R2PI spectra at the lowest possible pulse energies that still led to a measurable ion signal show a broad absorption band on which sharper bands are superimposed (Fig. S6). In (1 + 1′) R2PI experiments, on the other hand, pulse energies on the order of

10 μJ could be employed, which led to excitation spectra that only showed a hint of a background (Fig. S7). Initially we had hoped that PE spectra might provide further insight into such a coupling with a nearby excited state. On the basis of corresponding ionization continua, ionization of $^1n\pi^*$ character is expected to occur predominantly to the $(n)^{-1}$ ionic state. However, the energy of this state is higher than accessible in our $(1 + 1')$ ionization experiments, and this ionic state is thus not visible in the recorded PE spectra. On the other hand, if a strong coupling is present, this might also influence the relative contributions of the ionization pathways to D_0 and D_1. Comparison of the PE spectra of MS -for which such a coupling would not be present- and SML does not show any striking differences. We therefore conclude that $(1 + 1')$ ionization experiments at much higher ionization energies would be needed to elucidate to which extent coupling plays a role.

3.3. Methyl ferulate

In a recent study we have reported on experimental and theoretical studies of MF and its microsolvated cluster with water.[45] This compound is of considerable interest as it can be considered as being in between sinapates that have two *meta*-substituted methoxy groups and coumarates that do not have any *meta*-substituents. To put this in a further context: in sinapates, the $V(\pi\pi^*)$ state is vertically as well as adiabatically at lower energies than the $^1n\pi^*$ state while in coumarates the $^1n\pi^*$ state is adiabatically the lowest excited singlet state and serves as a highly effective doorway state for intersystem crossing (ISC) to the triplet manifold. Quantum chemical calculations predict that MF resembles in that respect MS as is indeed supported by the bi-exponential time dependence of measured time-resolved $(1 + 1')$ R2PI decay curves.[45] These studies found that under molecular beam conditions three conformers can be distinguished that are assigned to the *syn*/*cis*, *syn*/*trans* and *anti*/*trans* conformers. It is interesting to notice that for the *syn*/*cis*, *syn*/*trans* a slightly smaller contribution of the decay associated with the decay of the triplet state was observed than for MS, while for the *anti*/*trans* conformer this contribution was much larger.

Fig. 7 displays the (1 + 1) PE spectrum obtained for the *syn*/*cis* conformer after excitation of the $S_1 \leftarrow S_0$ 0-0 transition at 31 508.5 cm^{-1}, while Fig. S8 and S9 in the SI show similar spectra for the *syn*/*trans* and *anti*/*trans* conformers. Fig. 7 shows that at this excitation energy a two-photon level is reached that is barely above the adiabatic $D_0 \leftarrow S_0$ ionization energy. As a result well-resolved bands associated with ionization to vibrational levels in D_0 can be observed. In agreement with predicted Franck–Condon spectra for the $D_0 \leftarrow S_1$ transition and following what is observed in the ZEKE-PFI studies on MS[44] this vibrational activity pertains predominantly a progression of the in-plane C_4–C_7═C_8 bending mode at 61.5 cm^{-1} (7.62 meV). The observation of well-separated transitions to the vibrationless level of D_0 allows us to come to an accurate determination of the adiabatic $D_0 \leftarrow S_0$ ionization energy as 7.7742 ± 0.0005 eV. Comparison with the ionization energy of MS and SML (7.475 and 7.459 eV) thus shows that the absence of one of the *meta*-substituted methoxy groups increases the ionization energy by about 0.3 eV.

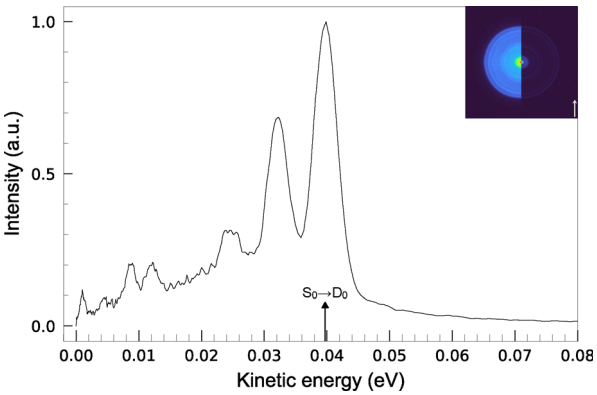

Fig. 7 PE spectrum of the *syn*/*cis* conformer of methyl ferulate obtained after one-colour (1 + 1) R2PI *via* the $S_1 \leftarrow S_0$ 0-0 transition at 31 508.5 cm^{-1}. The black arrow is the value of the kinetic energy taken to be associated with adiabatic $D_0 \leftarrow S_0$ ionization. The inset shows in the left half the recorded image while the right half presents the reconstructed slice through the centre of the original 3D distribution with the arrow indicating the electric field polarisation of the laser pulse.

From Fig. S8 we similarly determine for the *syn*/*trans* conformer a slightly higher ionization energy of 7.799± 0.001 eV, noticing as well a reduced Franck–Condon activity in the PE spectrum of the in-plane C_4–C_7═C_8 bending mode compared to the *syn*/*cis* conformer. For the *anti*/*trans* conformer (Fig. S9), on the other hand, the two-photon energy is at such a level that vibrational resolution is no longer observed. We can nevertheless still determine the adiabatic ionization energy reasonably accurately from the maximum of this band and thus find a value of 7.86± 0.01 eV.

PE spectra obtained for $(1 + 1')$ R2PI ionization of MF are reported in Fig. 8 for the *syn*/*cis* conformer and Fig. S10 and S11 for the *syn*/*trans* and *anti*/*trans* conformers, respectively. Similar to MS and SML these spectra show three bands that on the basis of their pump–probe dependence are assigned to the same ionization channels as concluded for MS and SML. Once again we find that the reorganization energy predicted to be associated with the $S_1 \leftarrow S_0$ transition (band I) is in good agreement with the observed value. As was observed as well for SML, we find for MF as well that the calculated $D_1 \leftarrow S_1$ ionization energy is slightly overestimated.

A further comparison of the $(1 + 1')$ spectrum of *syn*/*cis* MF with those of MS and SML reveals two differences. Firstly, the relative contribution of the $D_1 \leftarrow S_1$ ionization pathway (band II) is smaller in MF than in MS and SML. Following the previous discussion on these pathways in MS, this could either indicate a reduced vibronic coupling between the $V(\pi\pi^*)$ and $V'(\pi\pi^*)$ in MF or a reduced contribution of the $HOMO^0LUMO^1$ configuration to the wavefunction of D_1. Secondly, also the contribution of the $D_0 \leftarrow T_{1p}$ ionization pathway (band III) is reduced. Such an observation nicely agrees with our initial observation from time-resolved $(1 + 1')$ R2PI decay curves which suggested a reduced ISC yield. Similar observations are made for the *syn*/*trans* conformer (Fig. S10) although here the contribution of the

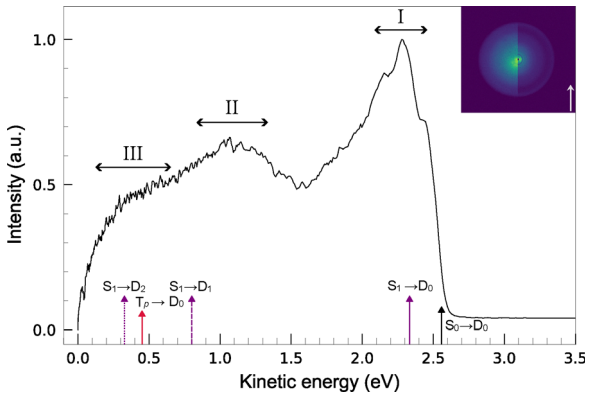

Fig. 8 PE spectrum of the *syn*/*cis* conformer of methyl ferulate obtained after two-colour (1 + 1′) R2PI *via* the $S_1 \leftarrow S_0$ transition at 31 508.5 cm^{-1} and using a 193 nm photon for ionization. The inset shows in the left half the recorded image while the right half presents the reconstructed slice through the centre of the original 3D distribution with the arrow indicating the electric field polarisation of the counter-propagating excitation and ionization laser pulses. The kinetic energy associated with adiabatic $D_0 \leftarrow S_0$ ionization as determined from the one-colour PE spectrum is indicated with the black solid arrow. Kinetic energies associated with transitions for electronically excited states are indicated by coloured arrows: purple for vertical ionization from the S_1 state, red for vertical ionization from the T_{1p} state. Line styles represent transitions to different states: solid lines to D_0, dashed lines to D_1, and dotted lines to D_2.

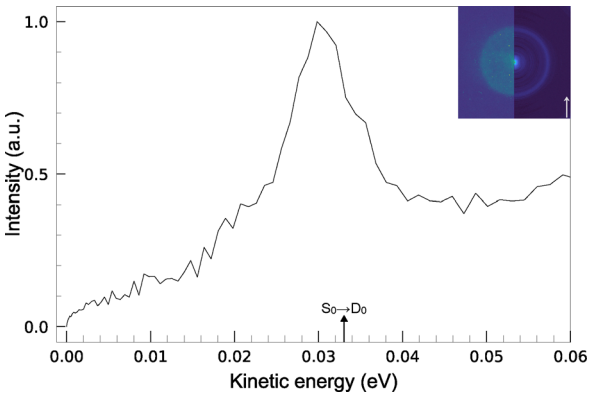

Fig. 9 PE spectrum of the *anti*/*cis* conformation of methyl coumarate obtained after one-colour (1 + 1) R2PI *via* the $S_1 \leftarrow S_0$ 0-0 transition at 32 710 cm^{-1}. The black arrow is the value of the kinetic energy expected from the adiabatic ionization energy determined from ionization efficiency spectra.[46] The inset shows in the left half the recorded image while the right half presents the reconstructed slice through the centre of the original 3D distribution with the arrow indicating the electric field polarisation of the laser pulse.

$D_1 \leftarrow S_1$ ionization pathway (band II) appears to be slightly larger. For the *anti*/*trans* conformer (Fig. S11), on the other hand, the contribution of the $D_0 \leftarrow T_{1p}$ ionization pathway (band III) is relatively larger as would have been expected on the basis of time-resolved (1 + 1′) R2PI decay curves.

3.4. Methyl coumarate

In previous R2PI studies[46,47] we have shown that one-color (1 + 1) ionization of MC *via* the S_1 state is quite inefficient. As a result relatively high laser powers need to be used in such experiments as a result of which the $S_1 \leftarrow S_0$ transition is strongly saturated, leading to significant power broadening of the excitation spectrum. We thus find that the (1 + 1) R2PI PE spectrum of the *anti*/*cis* conformer of MC (Fig. 9) is dominated by photoelectrons associated with non-resonant background ionization. We nevertheless also observe a sharp band at 0.030 eV. Such a band is in excellent agreement with a kinetic energy of 0.033 eV expected on the basis of the adiabatic $D_0 \leftarrow S_1$ ionization energy of this conformer determined from ionization efficiency spectra of the vibrationless level of S_1 (65 154 cm^{-1} (8.078 eV)).[26,46] We therefore take this band as indeed originating from the $D_0 \leftarrow S_1$ pathway of MS.

Two-color (1 + 1′) R2PI allows for much more efficient photoionization and leads to excitation spectra in which the signals are proportional to the power of the excitation laser. Fig. 10 displays the PE spectrum obtained after (1 + 1′) R2PI ionization of the MC *anti*/*cis* conformer *via* the $S_1 \leftarrow S_0$ transition at 32 710 cm^{-1}, which is illustrative as well for PE spectra observed for other MC conformers. The maximum photoelectron kinetic energy that is expected on the basis of the adiabatic $D_0 \leftarrow S_1$ ionization energy is ∼ 2.4 eV. However, at these kinetic energies no signals are observed.

The PE spectrum shown in Fig. 10 is distinctly different from PE spectra recorded for MS, SML, and MF. In the latter compounds clear signatures are observed of photoionization pathways originating from S_1 with a minor contribution from triplet associated ionization pathways. Fig. 10, on the other hand, displays a broad band that on the basis of its pump–probe delay dependence is assigned to $D_0 \leftarrow T_{1p}$ ionization. It is interesting to notice that in the case of MC an ionization pathway involving vertical ionization of the $^1n\pi^\star$ state to its $(n)^{-1}$

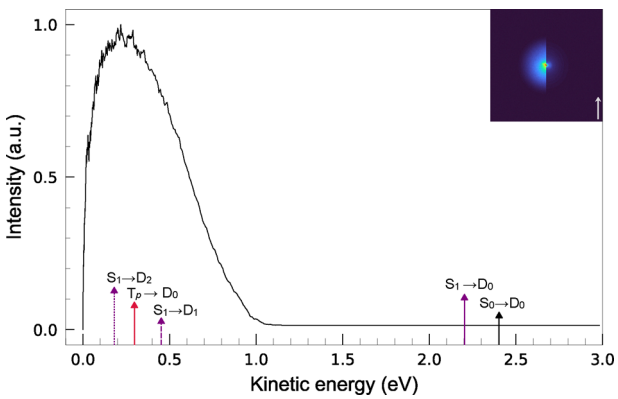

Fig. 10 PE spectrum of the *anti*/*cis* conformer of methyl coumarate obtained after two-colour (1 + 1′) R2PI *via* the $S_1 \leftarrow S_0$ transition at 32 710 cm^{-1} and using a 193 nm photon for ionization. The inset in the upper right corner shows in the left half the recorded image while the right half presents the reconstructed slice through the centre of the original 3D distribution with the arrow indicating the electric field polarisation of the counter-propagating excitation and ionization laser pulses. The kinetic energy associated with adiabatic $D_0 \leftarrow S_0$ ionization as determined from ionization efficiency spectra[46] is indicated with the black solid arrow. Kinetic energies associated with transitions for electronically excited states are indicated by coloured arrows: purple for vertical ionization from the S_1 state, red for vertical ionization from the T_{1p} state. Line styles represent transitions to different states: solid lines to D_0, dashed lines to D_1, and dotted lines to D_2.

corresponding ionization continuum is predicted to generate photoelectrons around 0.7 eV. Although the PE spectrum shows activity in this region, its time dependence does not give solid evidence for the presence of this pathway. Such a conclusion is in line with expectations based on PE spectra recorded with femtosecond lasers that do not show any distinct signatures of such a pathway either.[30] We thus conclude that in our R2PI experiments we effectively only observe ionization of the lowest triplet state. Such a conclusion is in agreement with $(1 + 1')$ R2PI decay curves recorded upon monitoring ions at the mass of the molecular ion since these show at all excitation energies a monoexponential decay with a time constant of about 30 ns.[47]

Conclusions

In the present work we have investigated the excited-state dynamics of a series of substituted cinnamates using one- and two-colour resonance enhanced two-photon ionization spectroscopy in combination with kinetic-energy-resolved photoelectron detection using velocity-map imaging of electrons. These cinnamates were chosen such as to reflect the various aspects that might come into play in determining these dynamics such as the ordering and relative energy differences of electronically excited states as well as the intrinsic electronic character of S_1. In combination with quantum chemical calculations, the photoelectron spectra (i) have led to an accurate determination of the adiabatic ionization energy of the ground state D_0 of the ion, but (ii) more importantly, have provided a direct view on the photoionization pathways along which these molecules are ionized after excitation of S_1, and thereby on the excited-state pathways along which the initially excited electronic state decays. Previously, the participation of a triplet-mediated pathway was convincingly but nevertheless only indirectly inferred from ionization efficiency spectra. One of the key contributions of the present studies is the direct observation of such a pathway.

For methyl sinapate, sinapoyl methyl lactate and methyl ferulate it was found that the triplet-mediated pathway plays a minor role, in agreement with the notion that for these compounds the V($\pi\pi^*$) state is both vertically as well as adiabatically S_1. As a result, intersystem crossing to the triplet manifold is relatively inefficient. Interestingly -and deviating from *a priori* expectations based on the concept of corresponding ionization continua- their $(1 + 1')$ photoelectron spectra show ionization to both D_0 as well as D_1 although the ionization efficiency to the latter is lower. As such, this observation underlines the multiconfigurational character of the electronically excited and ionic states of these compounds. Methyl coumarate, on the other hand, shows exclusively a triplet-mediated decay pathway. The dominance of this pathway can be attributed to a highly efficient intersystem crossing from an $^1n\pi^*$ state which adiabatically becomes the lowest electronically excited singlet state. The present studies thus confirm that near the energy minimum of the V($\pi\pi^*$) state, deactivation primarily takes place *via* internal conversion to the $^1n\pi^*$ state followed by intersystem crossing to the triplet manifold and decay of T_1 to the ground state. In view of the role of the $^1n\pi^*$ state -be it as doorway state for intersystem crossing in methyl coumarate, be it that adiabatically this state is in close proximity to the V($\pi\pi^*$) state in the other compounds- it would have been gratifying to observe some kind of involvement of this state in the photoionization dynamics. However, on the timescales and total absorbed energy of the present experiments such signatures could not be discerned in the recorded photoelectron spectra. Experiments on faster timescales and higher photoioniziation energies are in this respect highly interesting.

Our studies have provided further insight into the photophysics and photochemistry of this class of UV-filters that are used in commercial as well biological applications. As such, they pave the way for a further rational development of novel filters with targeted properties, for example, by judiciously chosen substitutions on the phenyl ring and/or adapting the tail involving the vinyl side chain. Such efforts, involving both studies under molecular beam as well as solution conditions, are presently underway.

Author contributions

W. R. designed the spectrometer and constructed it together with I. R. I. R. performed the spectroscopic experiments with the help of Y. B. and H. M. I. R. and W. J. B. performed the quantum chemical calculations. I. R. and W. J. B. conceived the study and analysed the data. W. J. B. supervised the work. All authors contributed to writing the manuscript.

Conflicts of interest

There are no conflicts to declare.

Data availability

Data for this article, including Fig. 1–10 and Fig. S1–S11, are available at Zenodo at **https://doi.org/10.5281/zenodo.15647305**.

Additional (1+1) and (1+1′) PE spectra of conformers of methyl sinapate, sinapoyl methyl lactate, and methyl ferrulate; Time-resolved (1+1′) R2PI curves of conformers of synapoyl methyl lactate; (1+1) and (1+1′) R2PI excitation spectra of sinapoyl methyl lactate. See DOI: **https://doi.org/10.1039/d5cp02240a**

Acknowledgements

This project has received funding from the European Unions Horizon 2020 research and innovation programme under the grant agreement No. 828753. We gratefully acknowledge drs. Hans Sanders for the synthesis of methyl sinapate and sinapoyl methyl lactate.

References

1 A. Chenu and G. D. Scholes, *Annu. Rev. Phys. Chem.*, 2015, **66**, 69–96.
2 T. Brixner, J. Stenger, H. M. Vaswani, M. Cho, R. E. Blankenship and G. R. Fleming, *Nature*, 2005, **434**, 625–628.
3 N. Koumura, R. W. J. Zijlstra, R. A. van Delden, N. Harada and B. L. Feringa, *Nature*, 1999, **401**, 152–155.
4 P. Roy, W. R. Browne, B. L. Feringa and S. R. Meech, *Nat. Commun.*, 2023, **14**, 1253.
5 I. Schapiro, M. Gueye, M. Paolino, S. Fusi, G. Marchand, S. Haacke, M. E. Martin, M. Huntress, V. P. Vysotskiy, V. Veryazov, J. Léonard and M. Olivucci, *Photochem. Photobiol. Sci.*, 2019, **18**, 2259–2269.
6 L. A. Baker, B. Marchetti, T. N. V. Karsili, V. G. Stavros and M. N. R. Ashfold, *Chem. Soc. Rev.*, 2017, **46**, 3770–3791.
7 X. Cui, Q. Ruan, X. Zhuo, X. Xia, J. Hu, R. Fu, Y. Li, J. Wang and H. Xu, *Chem. Rev.*, 2023, **123**, 6891–6952.
8 T. T. Abiola, B. Rioux, J. M. Toldo, J. Alarcan, J. M. Woolley, M. A. P. Turner, D. J. L. Coxon, M. Telles do Casal, C. Peyrot, M. M. Mention, W. J. Buma, M. N. R. Ashfold, A. Braeuning, M. Barbatti, V. G. Stavros and F. Allais, *Chem. Sci.*, 2021, **12**, 15239–15252.
9 E. M. M. Tan, M. Hilbers and W. J. Buma, *J. Phys. Chem. Lett.*, 2014, **5**, 2464–2468.
10 K. Hanson, E. Gratton and C. Bardeen, *Free Rad. Biol. Med.*, 2006, **41**, 1205–1212.
11 S. K. Allen, A. Todd and J. M. Allen, *Biochem. Biophys. Res. Commun.*, 1997, **235**, 615–618.
12 T. M. Karpkird, S. Wanichweacharungruang and B. Albinsson, *Photochem. Photobiol. Sci.*, 2009, **8**, 1455–1460.
13 M. Promkatkaew, S. Suramitr, T. M. Karpkird, S. Namuangruk, M. Ehara and S. Hannongbua, *J. Chem. Phys.*, 2009, **131**, 224306.
14 M. Promkatkaew, S. Suramitr, T. Karpkird, S. Wanichwecharungruang, M. Ehara and S. Hannongbua, *Photochem. Photobiol. Sci.*, 2014, **13**, 583–594.
15 J. C. Dean, R. Kusaka, P. S. Walsh, F. Allais and T. S. Zwier, *J. Am. Chem. Soc.*, 2014, **136**, 14780–14795.
16 T. N. V. Karsili, B. Marchetti, M. N. R. Ashfold and W. Domcke, *J. Phys. Chem. A*, 2014, **118**, 11999–12010.
17 X.-P. Chang, C.-X. Li, B.-B. Xie and G. Cui, *J. Phys. Chem. A*, 2015, **119**, 11488–11497.
18 L. A. Baker, M. D. Horbury, S. E. Greenough, F. Allais, P. S. Walsh, S. Habershon and V. G. Stavros, *J. Phys. Chem. Lett.*, 2016, **7**, 56–61.
19 X.-Y. Xie, C.-X. Li, Q. Fang and G. Cui, *J. Phys. Chem. A*, 2016, **120**, 6014–6022.
20 L. A. Baker, M. Staniforth, A. L. Flourat, F. Allais and V. G. Stavros, *ChemPhotoChem*, 2018, **2**, 743–748.
21 Y. Liu, X. Zhao, J. Luo and S. Yang, *J. Lumin.*, 2019, **206**, 469–473.
22 X. Zhao, J. Luo, Y. Liu, P. Pandey, S. Yang, D. Wei and K. Han, *J. Phys. Chem. Lett.*, 2019, **10**, 5244–5249.
23 X. Zhao, J. Luo, S. Yang and K. Han, *J. Phys. Chem. Lett.*, 2019, **10**, 4197–4202.
24 J. M. Toldo, M. T. do Casal and M. Barbatti, *J. Phys. Chem. A*, 2021, **125**, 5499–5508.
25 K. Yamazaki, Y. Miyazaki, Y. Harabuchi, T. Taketsugu, S. Maeda, Y. Inokuchi, S.-N. Kinoshita, M. Sumida, Y. Onitsuka, H. Kohguchi, M. Ehara and T. Ebatas, *J. Phys. Chem. Lett.*, 2016, **7**, 4001–4007.
26 S.-n Kinoshita, Y. Miyazaki, M. Sumida, Y. Onitsuka, H. Kohguchi, Y. Inokuchi, N. Akai, T. Shiraogawa, M. Ehara, K. Yamazaki, Y. Harabuchi, S. Maeda, T. Taketsugu and T. Ebata, *Phys. Chem. Chem. Phys.*, 2018, **20**, 17583–17598.
27 S.-n Kinoshita, Y. Inokuchi, Y. Onitsuka, H. Kohguchi, N. Akai, T. Shiraogawa, M. Ehara, K. Yamazaki, Y. Harabuchi, S. Maeda and T. Ebata, *Phys. Chem. Chem. Phys.*, 2019, **21**, 19755–19763.
28 S.-n Kinoshita, Y. Harabuchi, Y. Inokuchi, S. Maeda, M. Ehara, K. Yamazaki and T. Ebata, *Phys. Chem. Chem. Phys.*, 2021, **23**, 834–845.
29 S. Muramatsu, S. Nakayama, S.-N. Kinoshita, Y. Onitsuka, H. Kohguchi, Y. Inokuchi, C. Zhu and T. Ebata, *J. Phys. Chem. A*, 2020, **124**, 1272–1278.
30 J. Dalton, G. W. Richings, J. M. Woolley, T. T. Abiola, S. Habershon and V. G. Stavros, *Molecules*, 2021, **26**, 1–15.
31 A. T. J. B. Eppink and D. H. Parker, *Rev. Sci. Instrum.*, 1997, **68**, 3477–3484.
32 A. Vredenborg, W. G. Roeterdink and M. H. M. Janssen, *Rev. Sci. Instrum.*, 2008, **79**, 063108.
33 A. Edelstein, N. Amodaj, K. Hoover, R. Vale and N. Stuurman, *Curr. Protocols Mol. Biol.*, 2010, **92**, 14.20.1–14.20.17.
34 C. R. Harris, K. J. Millman, S. J. van der Walt, R. Gommers, P. Virtanen, D. Cournapeau, E. Wieser, J. Taylor, S. Berg, N. J. Smith, R. Kern, M. Picus, S. Hoyer, M. H. van Kerkwijk, M. Brett, A. Haldane, J. F. del Río, M. Wiebe, P. Peterson, P. Gérard-Marchant, K. Sheppard, T. Reddy, W. Weckesser, H. Abbasi, C. Gohlke and T. E. Oliphant, *Nature*, 2020, **585**, 357–362.
35 D. Hickstein, R. Yurchak, D. Das, C.-Y. Shih and S. Gibson, *PyAbel: A Python Package for Abel Transforms*, 2016, DOI: **10.5281/zenodo.47423**.
36 G. Van Rossum and F. L. Drake, Python 3 Reference Manual, CreateSpace, Scotts Valley, CA, 2009.
37 M. Ryazanov, PhD thesis, University of Southern California, Los Angeles, California, USA, 2012.
38 J.-D. Chai and M. Head-Gordon, *Phys. Chem. Chem. Phys.*, 2008, **10**, 6615–6620.
39 J. Dunning and H. Thom, *J. Chem. Phys.*, 1989, **90**, 1007–1023.
40 S. Kenjo, Y. Iida, N. Chaki, S. Nosuke Kinoshita, Y. Inokuchi, K. Yamazaki and T. Ebata, *Chem. Phys.*, 2018, **515**, 381–386.
41 M. J. Frisch, G. W. Trucks, H. B. Schlegel, G. E. Scuseria, M. A. Robb, J. R. Cheeseman, G. Scalmani, V. Barone, G. A. Petersson, H. Nakatsuji, X. Li, M. Caricato, A. V. Marenich, J. Bloino, B. G. Janesko, R. Gomperts, B. Mennucci, H. P. Hratchian, J. V. Ortiz, A. F. Izmaylov, J. L. Sonnenberg, D. Williams-Young, F. Ding, F. Lipparini, F. Egidi, J. Goings, B. Peng, A. Petrone, T. Henderson,

D. Ranasinghe, V. G. Zakrzewski, J. Gao, N. Rega, G. Zheng, W. Liang, M. Hada, M. Ehara, K. Toyota, R. Fukuda, J. Hasegawa, M. Ishida, T. Nakajima, Y. Honda, O. Kitao, H. Nakai, T. Vreven, K. Throssell, J. A. Montgomery, Jr., J. E. Peralta, F. Ogliaro, M. J. Bearpark, J. J. Heyd, E. N. Brothers, K. N. Kudin, V. N. Staroverov, T. A. Keith, R. Kobayashi, J. Normand, K. Raghavachari, A. P. Rendell, J. C. Burant, S. S. Iyengar, J. Tomasi, M. Cossi, J. M. Millam, M. Klene, C. Adamo, R. Cammi, J. W. Ochterski, R. L. Martin, K. Morokuma, O. Farkas, J. B. Foresman and D. J. Fox, *Gaussian 16 Revision A.03*, 2016, Gaussian Inc., Wallingford CT.

42 P. R. Tentscher, *Phys. Chem. Chem. Phys.*, 2024, **26**, 29552–29567.

43 J. Fan, W. Roeterdink and W. J. Buma, *Mol. Phys.*, 2021, **119**, e1825850.

44 J. Fan, L. Finazzi and W. Jan Buma, *Phys. Chem. Chem. Phys.*, 2022, **24**, 3984–3993.

45 I. Romanov, Y. Boeije, J. M. Toldo, M. T. Do Casal, M. Barbatti and W. J. Buma, *J. Phys. Chem. A*, 2025, **129**, 36–49.

46 S. Smolarek, A. Vdovin, E. M. M. Tan, M. de Groot and W. J. Buma, *Phys. Chem. Chem. Phys.*, 2011, **13**, 4393–4399.

47 E. M. M. Tan, S. Amirjalayer, B. H. Bakker and W. J. Buma, *Faraday Discuss.*, 2013, **163**, 321–340.